INFLUENCE OF LEAKAGE FLOWS ON HOT GAS INGRESS

Marios Patinios **Irvin L Ong** **James A Scobie**

Gary D Lock **Carl M Sangan**

Department of Mechanical Engineering
University of Bath
Bath, BA2 7AY
United Kingdom

ABSTRACT

One of the most important problems facing gas turbine designers today is the ingestion of hot mainstream gases into the wheel-space between the turbine disc (*rotor*) and its adjacent casing (*stator*). A rim seal is fitted at the periphery and a superposed sealant flow – typically fed through the bore of the stator - is used to prevent ingress. The majority of research studies investigating ingress do so in the absence of any leakage paths that exist throughout the engine's architecture. These inevitable pathways are found between the mating interfaces of adjacent pieces of hardware. In an environment where the turbine is subjected to aggressive thermal and centrifugal loading these interface gaps can be difficult to predict and the resulting leakage flows which pass through them even harder to account for.

This paper describes experimental results from a research facility which experimentally models hot gas ingestion into the wheel-space of an axial turbine stage. The facility was specifically designed to incorporate leakage flows through the stator disc; leakage flows were introduced axially through the stator shroud or directly underneath the vane carrier ring. Measurements of CO_2 gas concentration, static pressure and total pressure were used to examine the wheel-space flow structure with and without ingress from the mainstream gas-path. Data is presented for a simple axial-clearance rim-seal. The results support two distinct flow-structures, which are shown to be dependent on the mass-flow ratio of bore and leakage flows. Once the leakage flow was increased above a certain threshold, the flow structure is shown to transition from a classical Batchelor-type rotor-stator system to a vortex-dominated structure. The existence of a toroidal vortex immediately inboard of the outer rim-seal is shown to encourage ingestion.

1 INTRODUCTION

The secondary air system of a gas turbine distributes the cooling air extracted from the main-gas path at several axial locations in the compressor. This air flow is used to ventilate and cool critical turbine components and to balance the pressure thrust on the rotating discs in order to maintain acceptable bearing loads. As there is an associated performance penalty associated with this extraction, the management and efficient use of this valuable flow is critical to overall engine efficiency.

Ingress in gas turbines occurs when mainstream gas enters the wheel-space formed between stationary and rotating discs. A significant amount of cooling air is required to prevent the hot mainstream gases from causing damage to vulnerable, highly stressed components. Minimising these purge and leakage flows is one of the last remaining places where significant cooling flow reductions may be possible with design improvements. Engine designers use rim seals fitted at the periphery of the wheel-space to minimise the effects of ingress and reduce purge levels. Reduced coolant flow rates lead directly to higher thermodynamic efficiency, provided the coolant is returned to the flow-path without causing large mixing losses.

In a gas turbine the first-stage nozzle guide vanes (NGVs) are manufactured in segments; outer and inner bands are formed when the nozzle segments are assembled. As shown in Figure 1 [1], leakages exist between the inner support (or carrier) ring and the first stage nozzle row. This interface leakage, commonly referred to as *chordal hinge leakage*, has a significant contribution to the egress from the rim seal.

To minimize leakage, the nozzles are designed with a chordal hinge seal [2]. The chordal hinge is a straight line seal on the downstream face on the inner sidewall rail (see Figure 1). This hinge seats against the support ring and provides a straight seal on a curved surface, thus maintaining a constant seal when the nozzle rocks slightly. In addition, movements of the first stage nozzles are allowed by these seals when the inner support ring encounters thermal expansions. During turbine operation the chordal hinge seal proves insufficient to completely prevent leakage due to the warpage resulting from

non-uniform temperature distributions. Supplemental seals can be employed to reduce the leakage flow [3], but with increased complexity and cost. However the potential exists for these inevitable flows to be exploited to help reduce hot gas ingress due to their close proximity to the rim-seal.

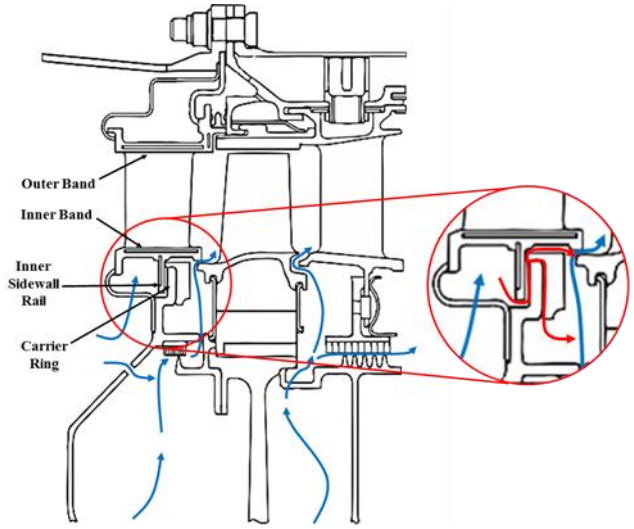

Figure 1: Sealing flow (blue arrows) and leakage flow (red arrows) paths in a typical turbine stage (adapted from [1])

This paper presents experimental measurements of ingress in the presence of leakage flows at the periphery of the wheel-space. An experimental facility was specifically adapted to incorporate leakage flows through the stator disc. Leakage flows are introduced axially through the stator shroud or directly underneath the vane carrier ring. Measurements of CO_2 gas concentration, static pressure and total pressure are used to examine the wheel-space flow structure, with and without ingress from the mainstream gas-path. Although leakage flows have been modelled in the past, and rigs designed to incorporate these flows experimentally, to the authors' knowledge this is the first study to give detail on the fluid dynamic effect of leakages with respect to hot gas ingress.

2 LITERATURE REVIEW

For a comprehensive review of ingress see Scobie *et al.* [4]. This review focusses on studies that incorporate leakage flows or consider the effect of the sealing inlet location on the fluid dynamics found in rotor-stator wheel-spaces.

Bunker [5] lists minimising leakage and purge flows as one of the ten remaining hot gas path challenges in gas turbines. It is explained that a secondary flow network is required to keep the hot working gases within the mainstream gas path. The secondary flow network must allow for component interfaces, accommodate differential growths and assembly and seal rotational boundaries. Where the secondary flow system meets the hot gas path there are necessary leakages and purge flows that can be minimised but not eliminated. Figure 2 identifies the different leakage flows present in the rim seal region including through the nozzle support which enter the turbine wheel-space.

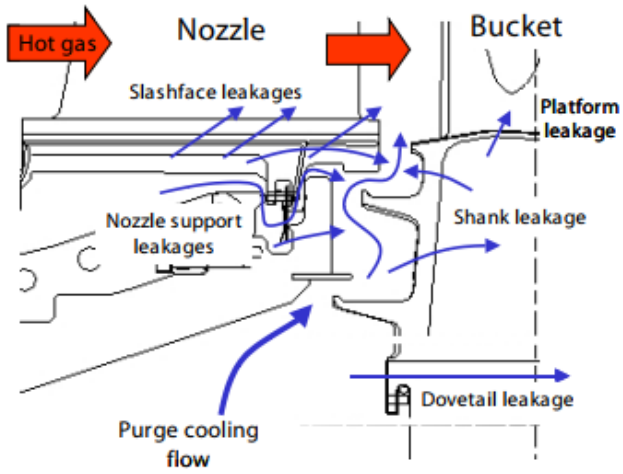

Figure 2: Interaction of purge and leakage flows in the rim seal region [5]

Andreini *et al.* [6] conducted a computational study on the effects of cooling supply geometry on a turbine stator-well configuration. Several cooling air supply geometries on the disc spacer arm were considered to determine the role of inlet angle, injection position and jet penetration on thermal effectiveness. The results demonstrate the effectiveness was increased when the inlet flow was angled both axially and tangentially as higher jet penetration is achieved. Similar improvements were also achieved when the inlet was re-positioned axially closer to the rotor disc.

Palafox *et al.* [7] present a rig capable of experimentally simulating the chordal hinge leakage flow. The 1.5-stage ingestion rig at the GE Global Research Centre is designed to operate at near engine conditions, including representative Mach and Reynolds numbers. Measurements of CO_2 gas concentration, unsteady pressure and temperature are possible. The chordal hinge flow was kept fixed at approximately 41% of the nominal purge level for the study, however the effect of this flow on ingress was not explored in detail within the paper. CFD validation of the preliminary rig data was presented by Ding *et al.* [8], who also incorporated the chordal hinge leakage flow in their computations.

Clark *et al.* [9] also investigated ingress into the wheel-space of a rig capable of engine-representative Mach and Reynolds numbers. Purge flow was introduced to the cavity through discrete holes for two different configurations: 150 and 32 purge holes. Sealing effectiveness measurements, again using CO_2 as a tracer gas, showed that the effectiveness was higher radially inward of the injection location with the increased hole configuration; radially outward of the injection location the sealing effectiveness was virtually independent of the number of holes used. The 32 hole configuration demonstrated a circumferential variation in concentration effectiveness near the inlet location for small sealing flow rates.

Zhang *et al.* [10] computationally investigated the introduction of sealing flow at various radial locations on the stationary surface of a stator-well cavity. The flow structure in the upstream stator-rotor wheel-space was shown to be

affected by the radial extent of the inlet. A counter-rotating vortex pair was shown to occur when the sealing flow impinged on the rotor surface. The outer vortex was strengthened and accelerated in the direction of the rotor disc pumping, whilst radially inward of the sealing injection point the vortex acted in the opposite direction.

3 EXPERIMENTAL FACILITY

The *Bath* one-stage axial turbine facility has been operational since 2009 and was originally designed for experimental investigations of hot gas ingress. The rig has been used extensively for measurements of heat transfer and fluid dynamics, validating a series of theoretical models (*e.g.* [11-14]. Recently the turbine stage was redesigned and reconfigured specifically for the introduction of leakage flows.

3.1 Test rig

The test section of the facility, shown in Figure 3, features a single turbine stage with 32 turned vanes and 41 symmetric blades. The stator disc, shroud and vanes were machined as a blisc, from a single piece of aluminium. The rotor blisc, which was similarly manufactured, could be rotated by an electric motor up to speeds of 3000 rpm. Owing to the symmetric design of the blades, no power was produced by the stage.

Compressed air was supplied to the turbine annulus through a radial diffuser, fed by a cylindrical pipe. 32 inlet pipes, each 25.4 mm in diameter, connected the radial diffuser to an annular transition upstream of the stator vanes. The annulus flow entering the turbine was measured using a calibrated orifice plate (built to EN ISO 5167-2 specifications). Further details of the supply system are documented extensively in [11].

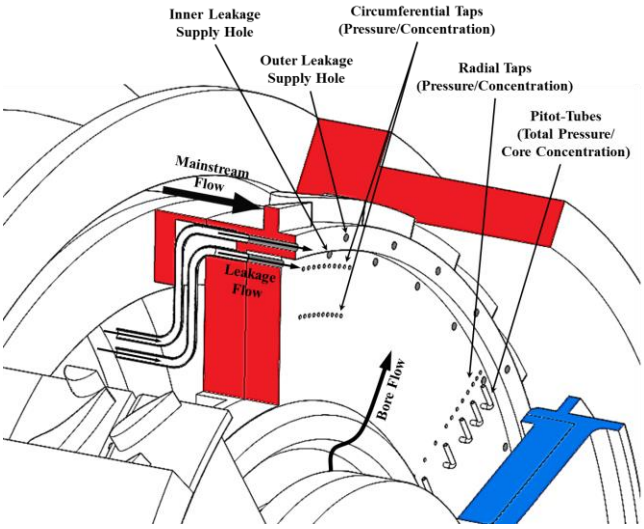

Figure 3: Test section and instrumentation of the 1-stage turbine rig

Secondary air was supplied to the wheel-space through the stator disc, both at low radius through the bore and at two high radius locations, one through the shroud and one immediately inboard of the shroud: these are termed *bore* flow, *inner leakage* flow and *outer leakage* flow, respectively. The leakage flows were supplied through a manifold which could be connected to *either* the 32 supply pipes in the stator shroud, at $r = r_{L,o}$, or 32 similar pipes immediately inboard of the shroud at $r = r_{L,i}$. The pipes, which were 3.28 mm in diameter, were positioned circumferentially at the midpoint between the vane leading edge and trailing edge and installed axially through the back of the stator disc (shown in Figure 3). The bore flow was supplied to the wheel-space through a low radius inlet seal. Thermal mass flow meters and close-coupled control valves were used to control the leakage ($\dot{m}_L$) and bore ($\dot{m}_B$) flows; all mass flows were measured to an accuracy of +/- 1% of the full-scale range. The leakage flow ranges were sized to be engine representative [15].

3.2 Operating conditions

Table 1 shows the operating conditions of the leakage flow facility. In this study experiments were conducted at 2500 rpm, creating a rotational Reynolds number Re_ϕ ~6 x 10^5. $Re_\phi \sim 10^7$ would be typical of modern engines, however the flow structure in rotor-stator systems is principally governed by the turbulent flow parameter, λ_T, and depends only weakly on Re_ϕ. In modern engines λ_T is typically less than 0.22 [16]; $\lambda_T < 0.3$ in all experiments presented here.

Parameter	Value
Rotational Reynolds Number, $\boldsymbol{Re_\phi}$	5.91×10^5
Axial Reynolds Number, $\boldsymbol{Re_w}$	3.18×10^5
Flow Coefficient, $\boldsymbol{C_F}$	0.538
Vane Exit Mach Number, $\boldsymbol{M}$	0.271

Table 1: Test rig operating conditions

The annulus mass-flow rate was matched to the disc speed so as to achieve an operating flow-coefficient, $C_F = 0.538$; the blades were unloaded at the design condition. The operating flow coefficient resulted in an axial Reynolds number, $Re_w = 3.18 \times 10^5$, and a corresponding Mach number at the vane exit plane of $M = 0.271$.

3.3 Experimental measurements

The distribution of static pressure, p, with radius ($0.66 < r/b < 0.99$) on the stator disc was measured through sampling ports of diameter 1.7 mm (see Figure 3). Five complementary Pitot tubes were installed in the wheel-space in order to measure the total pressure, p_T; the tubes were aligned to the tangential direction and proud of the stator disc at $z/S = 0.31$. The circumferential component of velocity in the core was resolved using Bernouilli's equation:

$$V_{\phi,\infty} = \left[\frac{2(p_T - p)}{\rho}\right]^{1/2} \tag{3.1}$$

where the density was based on values of pressure and temperature measured at entry to the wheel-space.

The swirl ratio of the fluid in the inviscid core is subsequently defined as

$$\beta = \frac{V_{\phi,\infty}}{\Omega r} \tag{3.2}$$

The circumferential distribution of pressure (*or* concentration) can also be measured on the stator wall using two sets of ten holes placed at two radial locations (r/b = 0.958; 0.85) and spanning a vane pitch of 11.25°. All pressure measurements were made using a 48-channel Scani-Valve, fitted with a differential pressure transducer with an accuracy of +/- 0.3% of the measurement range.

In order to monitor the mixing between the secondary air and ingress, the bore and leakage flows could be seeded with CO_2 tracer gas. The concentration of CO_2 was measured at the entrance to the wheel-space, c_B, in the leakage manifold, c_L, and in the unseeded turbine annulus immediately upstream of the stator vanes, c_a. The relative dilution of any seeded flow could be measured at 12 radial positions on the stator disc, c_s ($0.66 < r/b < 0.97$); the relative concentration was also measured at five discrete radial locations in the wheel-space at $z/S = 0.31$, c_∞, using the pitot tubes as inlets. Concentrations measurements were made using a dual-channel Signal Group 9000MGA gas analyser with repeatability and linearity of better than 1 % and 0.5 % of the full-scale range, respectively.

Detailed uncertainty analyses for the experimental variables used here are given in [13] and [17], for pressure-based and concentration-based parameters, respectively.

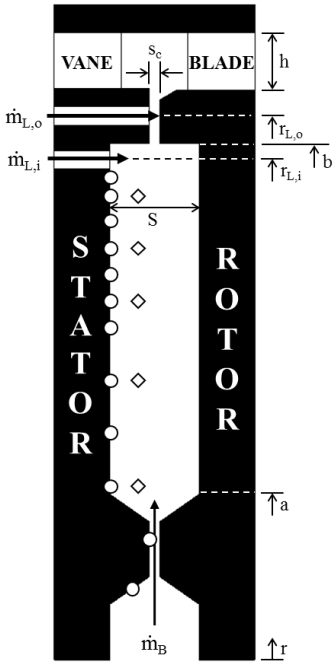

Figure 4: Axial seal configuration in the turbine wheel-space

3.4 Rim-seal configuration

A simple axial-clearance rim-seal configuration was formed between the stator and rotor shrouds at the periphery of the wheel-space (Figure 4); key parameters are annotated in the figure and shown in Table 2. The seal-clearance, s_c, used in Eqs. (3.3) and (3.4) is 2 mm; the seal clearance through the inlet seal is also 2 mm. The measurement locations described in Section 3.3 are shown on the stator disc and in the core as circles and diamonds on Figure 4, respectively.

Parameter	Dimension (mm)
h	10
s_c	2
S	16
a	122
b	185
$r_{L,o}$	190
$r_{L,i}$	182

Table 2: Dimensions for the stage configuration (nominal values under static conditions)

3.5 Measurements with dual superposed flows

Consider the control volume shown in Figure 5a for the case of a fully purged wheel-space (*i.e.* no ingress). The bore flow ($\dot{m}_B$) enters the wheel-space with concentration, c_B; similarly the leakage flow ($\dot{m}_L$) enters the system with concentration, c_L. After complete mixing in the rim-seal, all the superposed fluid leaves the system as egress flow with a mass-weighted average concentration, c_{egress}. Assuming that $c_B > c_L$, the relative dilution of c_B within the wheel-space would indicate incomplete mixing with the leakage flow; the local concentration was measured at various sampling ports on the stator, c_s. The dilution ratio, C^*, is defined as

$$C^* = \frac{(c_s - c_L)}{(c_B - c_L)} \tag{3.3}$$

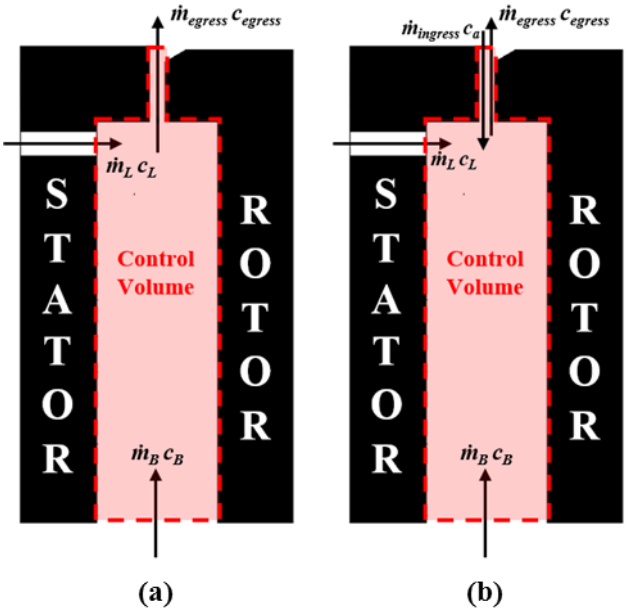

Figure 5: Representation of control volume for the case of: (a) no ingress and $c_B > c_L$ (b) with ingress and $c_B = c_L$.

Now consider the control volume shown in Figure 5b. In the case where ingress exists (*i.e.* the system is not purged), a mass-weighted concentration effectiveness is appropriate for the rim-seal:

$$\varepsilon_c = \frac{(c_s - c_a)(\dot{m}_B + \dot{m}_L)}{\dot{m}_B(c_B - c_a) + \dot{m}_L(c_L - c_a)} \tag{3.4}$$

In the special case where $c_B = c_L$, eq (3.4) reduces to

$$\varepsilon_c = \frac{(c_s - c_a)}{(c_B - c_a)} \equiv \frac{(c_s - c_a)}{(c_L - c_a)} \tag{3.5}$$

4 FLOW STRUCTURE IN ROTOR-STATOR SYSTEMS WITH LEAKAGE FLOWS

The flow structure in rotor-stator systems is well documented for conditions either *without* ingress (*e.g.* [16 & 18]) or *with* ingress (*e.g.* [19]). This section describes simplified flow structures for such systems with the addition of leakage flow.

4.1 Models of flow structure in rotor-stator systems

Figure 6 shows the simplified flow structure for a rotor-stator system with ingress; a superposed sealing flow is introduced to the system at low radius through the bore of the stator. The wheel-space gap ratio is large enough to ensure that separate boundary layers exist on the stator and rotor discs. Fluid moves radially outward in the boundary layer on the rotor and inward in the boundary layer on the stator. There is a gradual entrainment of flow from the stator to the rotor, axially across the rotating inviscid core that exists in the centre of the wheel-space. Due to the Taylor-Proudman theorem (see [18]) there are no axial gradients of the tangential and axial velocity components in the core and the radial component is zero; all radial flow is therefore confined to the boundary layers on the discs.

The superposed flow ($\dot{m}_B$) enters the system through the bore of the stator into an *inner region*, where all available flow is entrained by the rotor boundary layer. In the *outer region* the ingress and egress mix; this region is the source and sink for the stator and rotor boundary layers, respectively. Importantly, if the fluid is fully mixed in the outer region, the concentration – *and temperature in the case of an adiabatic stator* – of the fluid in the stator boundary layer, and that in the adjacent core, will be invariant with radius. This flow-structure is characteristically referred to as *Batchelor-type* flow [18].

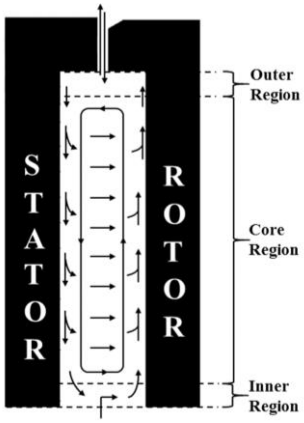

Figure 6: Simplified flow structure for a rotor-stator system with ingress and a superposed sealing flow

Figure 7a, which shows the expected flow structure where a small amount of leakage flow is introduced to the system ($\dot{m}_L < \dot{m}_B$), has similarities with Figure 6. The main difference is in the outer region, where the leakage flow moves axially across the wheel-space before exiting the system as egress.

Figure 7b shows the equivalent flow structure when $\dot{m}_L \geq \dot{m}_B$. Owing to the increased axial momentum in the leakage flow, a toroidal vortex is formed in the outer part of the wheel-space; the size of the vortex is dependent on the momentum flux ratio of the leakage flow. The rotating core is pushed radially inward by the vortex, forming an interface between the two. This flow structure is similar to that shown computationally by [10].

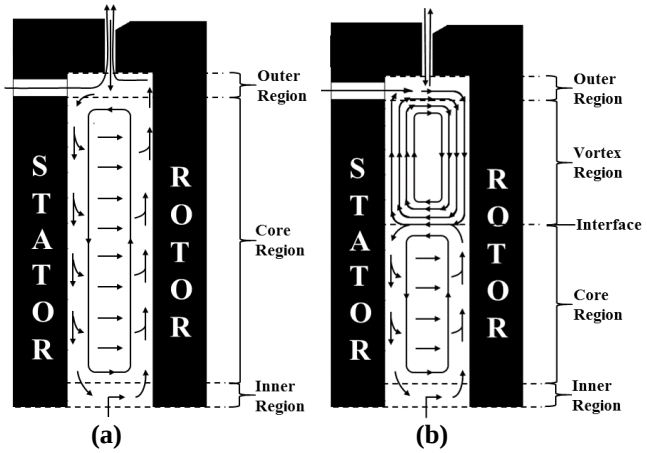

Figure 7: Simplified flow structures expected for a rotor-stator system with ingress, superposed sealing flow ($\dot{m}_B$) and leakage flow at high radius ($\dot{m}_L$): (a) $\dot{m}_L < \dot{m}_B$, (b) $\dot{m}_L \geq \dot{m}_B$

4.2 Some relevant non-dimensional parameters

The flow in a rotor-stator wheel-space is controlled by the viscous boundary-layers on the rotor and stator, whereas the ingestion of fluid into the system is an inviscid phenomenon. Some important modelling parameters relevant to this study are defined below.

Superposed flows

The non-dimensional sealing flow parameter, Φ, combines the effects of $\dot{m}$, s_c and Re_ϕ into a single variable:

$$\Phi = \frac{\dot{m}}{2\pi s_c \rho \Omega b^2} \tag{4.1}$$

The total superposed flow into the system, Φ_0, is equivalent to the sum of the bore and leakage flows:

$$\Phi_0 = \Phi_B + \Phi_L \tag{4.2}$$

where

$$\Phi_B = \frac{\dot{m}_B}{2\pi s_c \rho \Omega b^2} \tag{4.3}$$

and

$$\Phi_L = \frac{\dot{m}_L}{2\pi s_c \rho \Omega b^2} \tag{4.4}$$

The system is sealed if the sealing flow rate increases to Φ_{min}, the value of Φ_o required to prevent ingress.

The ratio of the superposed flows, $R_{\dot{m}}$, is given as follows:

$$R_{\dot{m}} = \frac{\Phi_L}{\Phi_B} \tag{4.5}$$

Wheel-space parameters

The structure of the flow in the wheel-space is determined by the turbulent flow parameter, which is defined as

$$\lambda_T = \frac{\dot{m}}{\mu b} Re_\phi^{-0.8} \tag{4.6}$$

For the free disc, where there is no stator, the entrained flow rate is characterised by $\lambda_{T,fd} \approx 0.22$. In a wheel-space, values of $\lambda_T > \lambda_{T,fd}$ are expected to suppress the core rotation.

It follows from eqs (4.1) and (4.6) that

$$\lambda_T = 2\pi G_c Re_\phi^{0.2} \Phi \quad (4.7)$$

where the subscripts, *0*, *B* and *L* can again be used to distinguish the *total*, *bore* and *leakage* flow components, respectively.

5 MEASUREMENTS WITHOUT INGRESS

In this section, the flow structure in the wheel-space is reported, exclusively for test conditions where ingress did not occur (*i.e.* $\Phi_0 \geq \Phi_{min}$). Experiments were conducted to investigate the interaction effects of *bore* and *leakage* flows. The bore flow was seeded with 1% CO_2 (c_B = 0.01); the leakage flow was unseeded but with an inherent concentration (c_L = 0.0004) measured in the supply manifold. Leakage flow is introduced here at the *inner* leakage location at $r = r_{L,i}$.

5.1 Radial distribution of effectiveness and pressure

Figure 8 shows the radial variation of C^*. The measurements were taken on the stator wall (circle symbols) and also in the rotating core (diamond symbols) using the pitot tubes described in Section 3.1. A silhouette of the seal is included alongside the figures, aligned with the radial position in the ordinate. The experiments were conducted at a fixed value of $\Phi_0 = 0.25$; in all cases ingress did not occur ($\Phi_0 > \Phi_{min}$). The ratio of superposed flows, $R_{\dot{m}}$, was varied by controlling the relative mass-flow rate of the leakage and bore flows. Data for $R_{\dot{m}} < 1$ is shown in Fig. 8a; data for $R_{\dot{m}} \geq 1$ is shown in Fig. 8b. The vertical dashed lines indicate the theoretical fully-mixed concentration in each case (c_{egress} in Fig. 5a).

Considering the left-hand-side of Figure 8a, it can be seen that the dilution ratio, C^*, measured on the stator and in the rotating core is broadly invariant with radius for $r/b \geq 0.66$. In all cases the dilution ratio in the rotating core is found to be approximately equal to that of the stator boundary layer. As illustrated in Fig. 7a, the source of the stator boundary layer is the *outer region*, where the flow is fully mixed; inboard of the outer region no further mass enters the stator boundary layer. The leakage flow directly exits the system through the rim-seal for conditions where $R_{\dot{m}} < 1$, resulting in a *bore-flow-dominated regime*. The flow structure is therefore expected to resemble classical Batchelor-type flow (see Section 4.1).

The right-hand-side of Fig. 8a shows the radial distribution of pressure in the wheel-space, shown in the form of a non-dimensional pressure coefficient:

$$C_p = \frac{p - p_{ref}}{1/2 \rho \Omega^2 b^2} \quad (5.1)$$

where p_{ref} is the pressure at r/b = 0.668. The distribution is consistent with Batchelor-type flow, where the radial gradient of pressure is determined by the radial distribution of swirl in the rotating inviscid core. For a rotating inviscid core, the radial momentum equation reduces to a balance between the pressure force and the centripetal acceleration so that

$$\frac{1}{\rho}\frac{dp}{dr} = \frac{V_\phi^2}{r} \quad (5.2)$$

The data in Figure 8b are for conditions where $R_{\dot{m}} \geq 1$. Considering the left-hand-side, it can be seen that the dilution ratio, C^*, measured on the stator and in the rotating core is approximately equal for $r/b \leq 0.85$. For $r/b > 0.85$ it can be seen that the core measurements exhibit increased dilution compared to the complementary taps on the stator wall. The difference in concentration between the taps at z/S = 0.31 and those on the stator wall are indicative of the rotating core being pushed radially inward, with the *unseeded* leakage flow being swept up into the toroidal vortex and diluting the *seeded* bore flow at high radius. The effect of the leakage flow being increased is significant and has changed the flow structure towards a *vortex-dominated regime* (sketched on the silhouette of the seal); this hypothesized flow structure was introduced in Section 4.1.

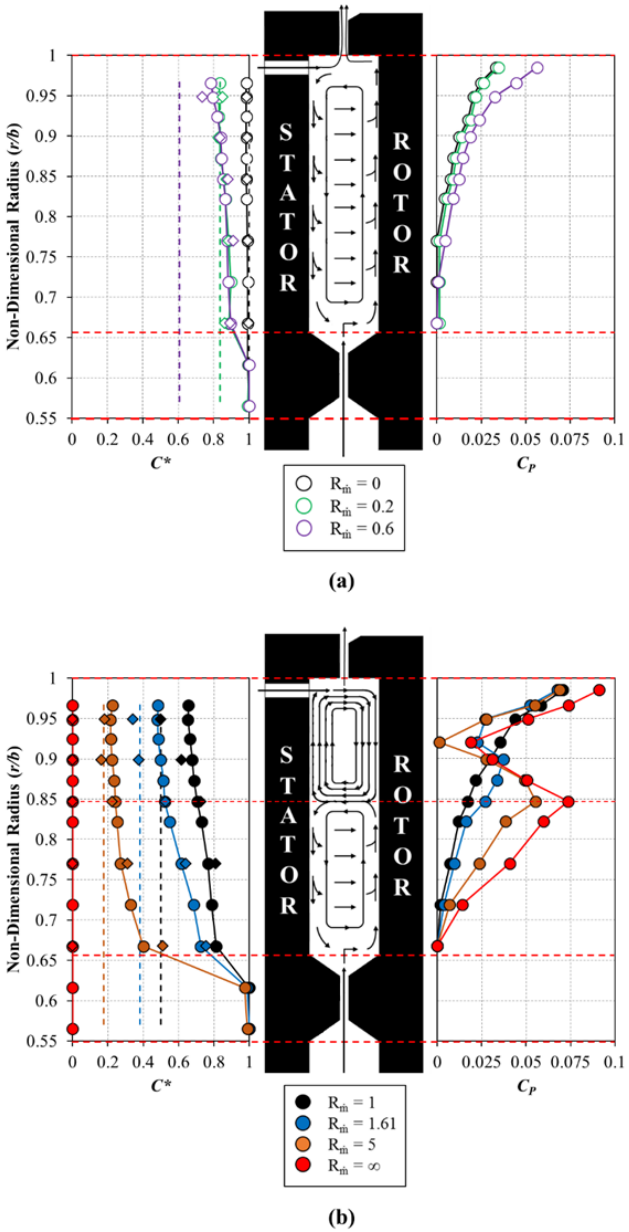

Figure 8: Effect of $R_{\dot{m}}$ on radial distribution of C^* (left) and C_p (right): (a) $R_{\dot{m}} < 1$ (b) $R_{\dot{m}} \geq 1$ (circles - stator wall; diamonds: rotating core) ($\Phi_0 = 0.25$)

Further evidence of the vortex-dominated regime is seen on the right-hand-side of Figure 8b. The radial distribution of pressure for $R_{\dot{m}} \geq 1$ progressively resembles that expected of

a toroidal vortex, where the low-pressure region at the centre of the vortex is seen to be at $r/b \approx 0.92$. The radial extent of the vortex spans $0.85 < r/b < 1$, with an interface occurring at $r/b \approx 0.85$; radially inward of the interface the flow structure returns to the Batchelor-type flow structure.

6 MEASUREMENTS WITH INGRESS

In this section, data is presented for experimental conditions where ingress does occur (*i.e.* $\Phi_0 < \Phi_{min}$). Experiments were conducted to investigate the interaction effects of the bore and leakage flows *with ingress*. The bore and leakage flows were both independently seeded with 1% CO_2 ($c_B = c_L = 0.01$); the annulus flow was unseeded but with an inherent concentration ($c_a = 0.0004$) measured in the turbine annulus upstream of the stator vanes. In all experiments reported here the concentration-based effectiveness was calculated using Eq (3.5). Leakage flow is introduced here at the *inner* leakage location at $r = r_{L,i}$.

6.1 Circumferential distribution of effectiveness

Figure 9 shows the circumferential variation of concentration effectiveness, ε_c, across a non-dimensional vane pitch, θ (shown in Fig. 3). The data is presented for two radial locations, $r/b = 0.85$ (shaded symbols) and 0.958 (open symbols), in the wheel-space. Results are shown for the following cases: bore flow only ($\Phi_B = 0.127$), leakage flow only ($\Phi_L = 0.127$) and a combined supply; for all cases the total superposed flow, $\Phi_0 = 0.127$.

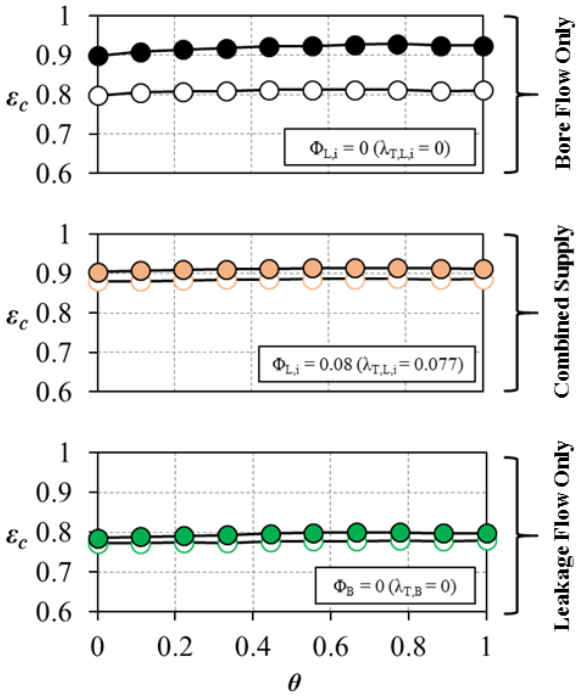

Figure 9: Circumferential variation of concentration effectiveness for the following cases: *bore flow only*, *leakage flow only* and a *combined supply*; in all cases Φ_0 = 0.127. (r/b = 0.85 (shaded symbols) and r/b = 0.958 (open symbols))

In all cases the effectiveness is shown to be invariant with circumferential location. This suggests that the flow in the wheel-space is axisymmetric and that any time-averaged influence of the discrete leakage supply holes is not sensed by the stator.

The consistency in ε_c between the two radial locations for the *leakage flow only* and *combined supply* conditions indicates that the effectiveness is invariant with radius for these cases. The reduction in effectiveness with radius for the *bore flow only* case implies that there is incomplete mixing in the outer region (see Figure 6) and that a small concentration gradient exists in the stator boundary layer. The radial distribution of ε_c in the wheel-space is discussed in more detail in Section 6.3.

6.2 Radial distribution of pressure and swirl

Figure 10 shows the radial distribution of non-dimensional pressure coefficient in the wheel-space. The tests were performed for a range of $\lambda_{T,0}$ (and hence Φ_0) values for the following cases: (a) *bore flow only*, (b) *combined supply*, and (c) *leakage flow only*. For reference, a silhouette of seal geometry is set alongside each figure. The measurement points for the total pressure (used in the calculation of C_p) are also shown on the silhouettes (diamond symbols).

As discussed in Section 5.1 for cases with no ingress, the radial gradient of pressure is determined by the radial distribution of swirl according to the radial momentum equation, Eq (5.2). Using the definitions of C_p and β in Section 3, Eq (5.2) can be integrated to give

$$C_p = \frac{p - p_{ref}}{0.5\rho\Omega^2 b^2} = 2\int_{x_{ref}}^{x} x\beta^2 dx \qquad (6.1)$$

where p_{ref} is the pressure at $r/b = x_{ref} = 0.668$. The numerical integration was carried out using Simpson's rule, with values of β calculated using Eqs (3.1) and (3.2) and a least-squares cubic spline fitted to the experimental data. The values of p_T and β are omitted here in the interest of brevity, with the final calculated values of C_p shown instead; the calculated values of C_p are plotted against measured values of C_p obtained from static pressure measurements in Figure 10.

Consider first the case with *bore flow only* (Fig 10a). For all $\lambda_{T,0}$ (and hence Φ_0) values there is good agreement between the calculated and measured values of C_p. This shows two important things: (*i*) the distribution of pressure is governed by $\lambda_{T,0}$; (*ii*) the radial distribution of pressure is consistent with an inviscid rotating core, characteristic of Batchelor-type flow. The data are similar in profile to the bore flow only case shown in Fig. 8a, for a comparable case *without* ingress. The flow structure is therefore assumed to be similar and consistent with the so-termed: *bore-flow-dominated regime*.

Now consider the *combined supply* case (Fig 10b); the $\lambda_{T,0} = 0$ data from Fig. 10a are reproduced here to aid comparison. Data for two combined supply cases are presented, both with a fixed value of leakage flow, $\lambda_{T,L,i} = 0.077$. The combined supply data are seen to deviate from the calculated distribution of C_p at high radius, consistent with the wheel-space flow structure transitioning from the conventional Batchelor-type flow ('bore-flow-dominated regime') towards the previously termed: *vortex-dominated regime*. Broad agreement between the measured and calculated values of C_p still exists at values of $r/b < 0.9$, suggesting the existence of a conventional Batchelor-type flow structure radially inward of this point.

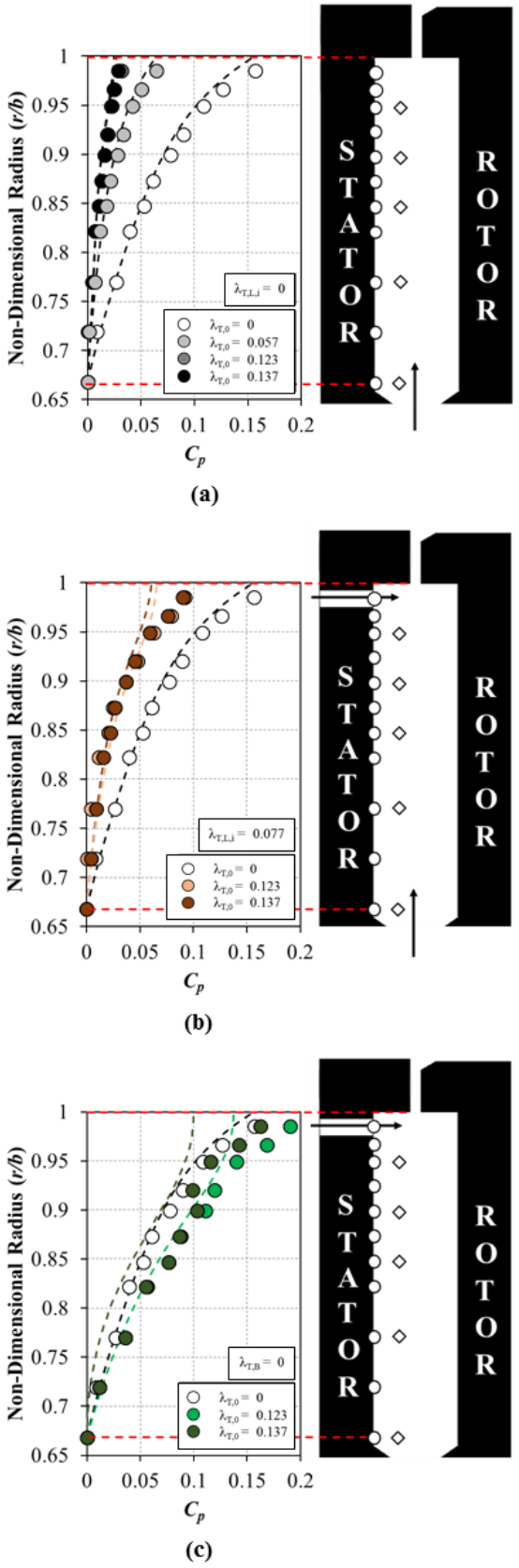

Figure 10: Effect of sealing flow rate on radial distribution of pressure coefficient for the following cases: (a) bore flow only, (b) combined supply and (c) leakage flow only – symbols: experimental measurements; lines: calculated distribution of C_p

The full transition to a vortex-dominated regime is more pronounced when considering the data shown in Fig. 10c for the *leakage flow only* case. Here, agreement with the calculated distribution of C_p is poor for all *r/b* values. As the leakage flow rate is increased the distribution of C_p with radius exhibits an inflection point (similar to those seen in Figure 8 at $r/b \approx 0.92$). The inflection point is characteristic of a toroidal vortex forming in the outer wheel-space and suggests the transition to a vortex-dominated regime has taken place. The case of $\lambda_{T,0} = 0.137$ is directly comparable to the $R_{\dot{m}} = 1.61$ case presented in Figure 8 - *for the fully sealed case with no ingress* - with both datasets consistently indicating a similar distribution of pressure.

6.3 Radial distribution of effectiveness

Figure 11 shows the radial variation of ε_c on the stator surface (circles) and at $z/S = 0.31$ (diamonds). In these experiments the sealing flow was supplied through the bore only, for two values of Φ_0. The effectiveness is shown to increase, in both the core and on the stator wall, as Φ_0 increases and the superposed flow raises the pressure in wheel-space relative to the annulus. In all cases the effectiveness in the rotating core is found to be consistent with the complementary measurement on the stator wall at consistent *r/b*. This distribution is similar to that shown in Figure 8a for the *bore-flow-dominated regime* that exists when $R_{\dot{m}} < 1$. Both data sets indicate the presence of a *Batchelor-type* flow structure where the stator boundary layer supplies fluid to the rotating core that exists in the centre of the wheel-space (hence $c_s \approx c_\infty$).

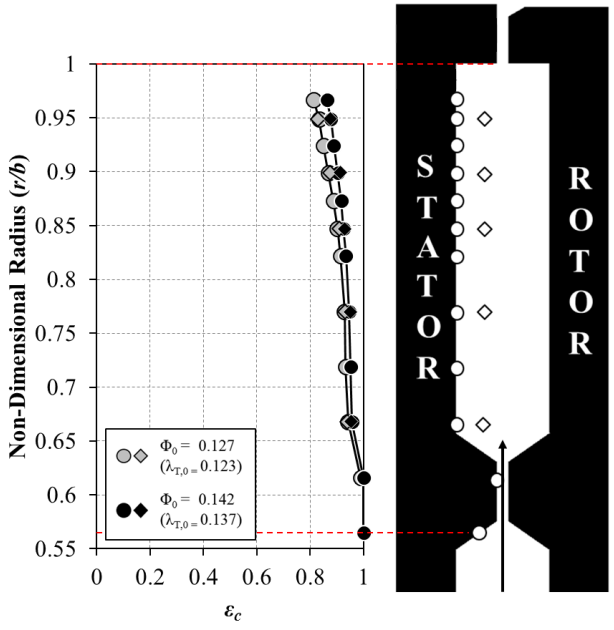

Figure 11: Effect of sealing flow rate on radial distribution of effectiveness for the *bore flow only* case – circles: stator wall; diamonds: measurements at z/S = 0.3125

In the case of fully mixed flow in the outer region (see Figure 6), the concentration in the stator boundary layer will be invariant radially inward of this point. The data in Figure

11 show a gradual decrease in effectiveness for $r/b > 0.8$, suggesting incomplete mixing in the stator boundary layer. For $0.8 \leq r/b \leq 0.668$, ε_c is broadly invariant with radius and no further mixing occurs in the stator boundary layer. Below $r/b = 0.668$ an abrupt increase in effectiveness is observed due to the presence of the inlet seal. This behaviour is consistent with data discussed in Section 6.1 and with previous work from the authors with regards axial-clearance seals (*e.g.* [4] & [11]).

As discussed above, the concentration in the core will be equal to that on the stator wall for conditions where a Batchelor-type flow structure exists. The absolute difference between measurements of effectiveness on the stator wall and those in the core at the same radius is given is follows

$$|\Delta\varepsilon_c| = \varepsilon_{c,s} - \varepsilon_{c,\infty} \qquad (6.2)$$

where $\varepsilon_{c,s}$ is the concentration effectiveness on the stator wall (based on c_s) and $\varepsilon_{c,\infty}$ is the concentration effectiveness at $z/S = 0.31$ (based on c_∞).

Figure 12 shows the radial distribution of $|\Delta\varepsilon_c|$ for the *bore flow only*, *combined supply* and *leakage flow only* cases. Experiments were conducted at two Φ_0 (and hence $\lambda_{T,0}$) values for each arrangement. Data for the *bore flow only* case (shown in Figure 11) are reproduced here in order to aid comparison; for both Φ_0 values the magnitude of $|\Delta\varepsilon_c|$ is close to zero and the distribution of $|\Delta\varepsilon_c|$ is broadly invariant with radius.

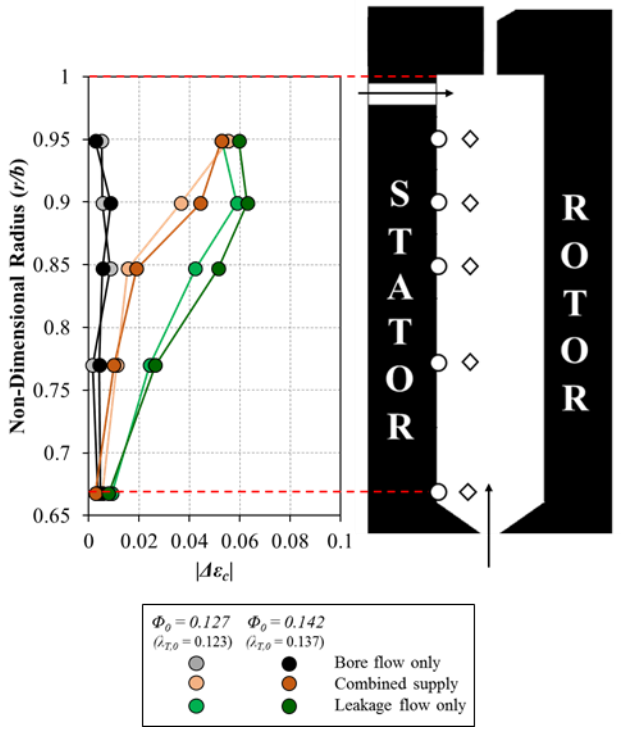

Figure 12: Effect of sealing supply arrangement on radial distribution of $|\Delta\varepsilon_c|$

Now consider the *combined supply* and *leakage flow only* arrangements. For both cases the magnitude of $|\Delta\varepsilon_c|$ is shown to increase with radius; at high radius this difference is as high as 6%. The difference in concentration effectiveness at high radius indicates a departure from the classical *Batchelor-type* flow structure. This evidence is consistent with the pressure data documented in Section 6.2, where it was postulated that a change in the flow structure had occurred with the introduction of leakage flow. It was suggested that the superposition of leakage flow into the bore-flow-dominated system had changed the flow structure towards a vortex-dominated regime, where a toroidal vortex exists at high radius.

The radial extent of this toroidal vortex can be visualised as the divergence point of the core and stator wall effectiveness measurements (*i.e.* when $d|\Delta\varepsilon_c|/dr >> 0$). The *leakage flow only* case diverges at lower radius (at $r/b \approx 0.66$) than the *combined supply* case (at $r/b \approx 0.85$), indicating a larger vortex with the former setup. The increased momentum in the *leakage only* case (where $\Phi_0 = \Phi_L$) promotes the formation of a larger, and potentially stronger, vortex.

6.4 Variation of effectiveness with sealing flow

Figure 13 shows the variation of ε_c with Φ_0 for the following cases: *bore flow only*, *leakage flow only* and a range of *combined supplies*. For the three combined supply cases the leakage flow component was kept constant at values of $\Phi_{L,i} = 0.03$, 0.08 and 0.12 (representing ~15%, ~40% and ~60% of the minimum amount of sealing flow, Φ_{min}, required to seal the system, respectively). The measurements were taken on the stator wall at $r/b = 0.847$. Leakage flow is introduced here at the *inner* leakage location at $r = r_{L,i}$.

Consider first the *bore flow only* case. The concentration effectiveness increases with Φ_0 (which is equal to Φ_B here) as the bore flow pressurises the wheel-space and reduces ingestion. The value of Φ_{min} is approximately 0.2. The shape of the Φ_0 versus ε_c curve is typical of those collected by the authors for similar axial seal configurations (*e.g.* those presented in [4] and [11]).

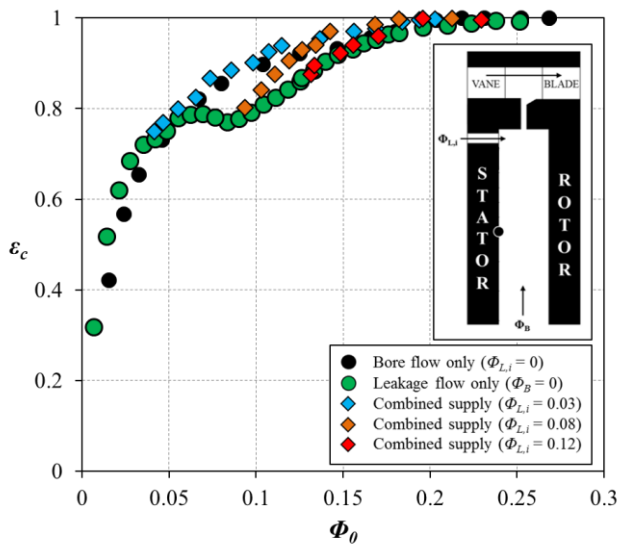

Figure 13: Variation of ε_c with Φ_0 at $r/b = 0.847$ for the *bore flow only*, *leakage flow only* and three *combined supply* cases

Now consider the other extreme where $\Phi_0 = \Phi_L$ (*i.e.* the *leakage flow only* case). The variation of ε_c with Φ_0 is markedly different here and exhibits a pronounced '*kink*' over

the range of Φ_0 values: $0.05 < \Phi_0 < 0.15$. For $\Phi_0 < 0.05$ the data is shown to collapse onto the *bore flow only* case; here the leakage flow is small and the structure is expected to resemble that of Batchelor-type flow (Figure 7a). Once the leakage flow reaches a certain level ($\Phi_0 = \Phi_L \approx 0.05$) the '*kink*' occurs and the flow structure is expected to resemble that of the *vortex-dominated regime* (Figure 7b). The range of Φ_0 over which the flow structure is expected to transition is consistent with the data shown in Sections 6.2 and 6.3. As Φ_0 is increased above 0.15, the data return to the trend of the *bore flow only* case and Φ_{min} is retained at approximately 0.2.

The cases where a *combined supply* (*i.e.* $\Phi_0 = \Phi_L + \Phi_B$) is delivered to the wheel-space are bounded by the two extremes. The first case of $\Phi_L = 0.03$ follows the trend of the *bore flow only* case. As the leakage flow component is increased further ($\Phi_L = 0.08$) the variation of ε_c with Φ_0 tends toward the *leakage flow only* case; once Φ_L is increased to 0.12 the data closely resemble the *leakage flow only* case.

Importantly, over the intermediate range of Φ_0 values the difference in ε_c between the *bore only* and *leakage-dominated* configurations could be greater than 10%.

6.5 Effect of leakage flow supply radius

All data presented prior to this point were for the *inner* leakage flow supply points at $r = r_{L,i}$. As discussed in Section 3.1, the supply manifold could be reconnected at a higher radius in the stator shroud; *outer* leakage flow through the shroud was introduced at $r = r_{L,o}$. Figure 14 shows the variation of ε_c with Φ_0 for the *outer* leakage flow case, where $\Phi_0 = \Phi_{L,o}$; data for the *inner* leakage flow case (where $\Phi_0 = \Phi_{L,i}$) and for the *bore flow only* case (where $\Phi_0 = \Phi_B$) are reproduced here from Figure 13 to aid comparison. The measurements of ε_c were taken on the stator wall at $r/b = 0.847$.

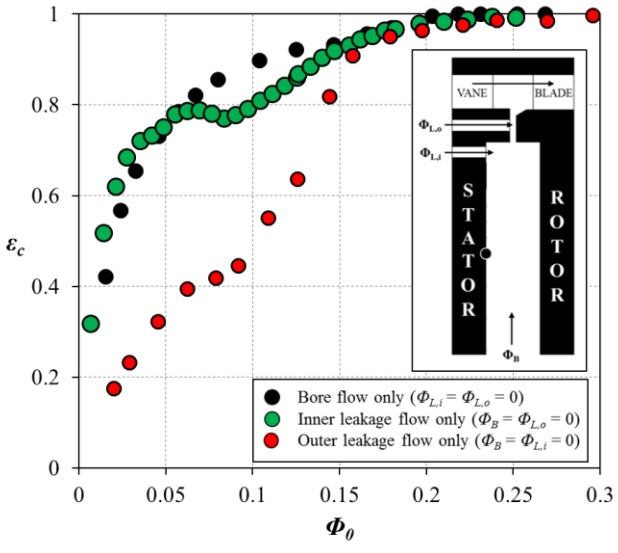

Figure 14: Effect of leakage flow supply radius on the variation of ε_c with Φ_0 (data measured at $r/b = 0.847$)

The data for the *outer* leakage flow radius exhibit a similar, albeit more pronounced, '*kink*' in the ε_c with Φ_0 curve over the range $0.05 < \Phi_0 < 0.15$. A similar vortex-dominated flow structure is expected to occur here radially inward of the rim-seal. While the Φ_{min} is once more retained at approximately 0.2, the effectiveness values for $\Phi_0 < 0.15$ are substantially lower than for the *inner* leakage flow and *bore flow only* cases. This reduction in effectiveness is as large as 40% and would represent a potentially catastrophic deterioration in rim-seal performance in the engine. It is postulated that the flow introduced to the system at high radius exits the rim-seal more readily than instead entering the rotor-stator cavity, resulting in delayed pressurisation of the wheel-space.

7 CONCLUSIONS

This paper describes a versatile one-stage axial turbine facility, specifically designed for the investigation of leakage flows and their effect on hot gas ingestion. The test rig, which models the fluid dynamics within the turbine wheel-space, allows for secondary air to be introduced through the stator bore, stator disc or stator shroud.

Measurements of static and total pressure were used to assess the fluid swirl in the centre of the wheel-space and the distribution of C_p, a non-dimensional pressure coefficient, on the stator wall. In the absence of ingress, the radial distribution of pressure at various ratios of leakage flow to bore flow, $R_{\dot{m}}$, identified two flow regimes: a *bore-flow-dominated* regime and a *vortex-dominated* regime. At low values of $R_{\dot{m}}$ the flow structure was shown to resemble classical Batchelor-type flow; at high values of $R_{\dot{m}}$ the flow structure was dominated by a toroidal vortex forming at high radius in the wheel-space.

Experiments *with ingress* identified similar flow structures to those *without ingress*: the wheel-space gradually transitioned from a bore-flow dominated regime to a vortex-dominated regime as the leakage flow was increased. Measurements of sealing effectiveness, using a CO_2 tracer gas in the bore and leakage flows, identified the radial extent of the toroidal vortex, which deepened with increasing leakage flow-rate. Once the leakage flow reached a certain level, the sealing effectiveness fell below that of the bore flow only supply; depending on flow rate this difference was shown to be as large as 10%.

Measurements of sealing effectiveness when the leakage flow supply was delivered at high radius through the stator shroud showed a further reduction in sealing performance. Compared to the leakage flow supply through the stator disc this further reduction in performance could be as high as 40%.

ACKNOWLEDGMENTS

The authors would like to thank John Maltson and Peter Smith, both at Siemens Industrial Turbomachinery Ltd., for their technical advice during the experimental programme.

NOMENCLATURE

b	radius of seal (m)
c	concentration of tracer gas ($\%$)
C^*	dilution ratio ($= (c_s\text{-}c_L)/(c_B\text{-}c_L)$)
C_F	flow coefficient ($= W/\Omega b$)
C_p	pressure coefficient ($= (p\text{-}p_{ref})/0.5\rho\Omega^2 b^2$)
G_c	seal-clearance ratio ($= s_c/b$)
h	height of annulus (m)

$\dot{m}$	mass flow rate (kg/s)
M	Mach number
p	absolute static pressure (Pa)
p_t	total pressure (Pa)
r	radius (m)
$R_{\dot{m}}$	ratio of superposed flows ($= \Phi_L/\Phi_B$)
Re_w	axial Reynolds number in annulus based on radius ($= \rho Wb/\mu$)
Re_ϕ	rotational Reynolds number ($= \rho\Omega b^2/\mu$)
s_c	seal clearance (m)
S	axial clearance between rotor and stator (m)
V_ϕ	tangential component of velocity (m/s)
W	axial velocity in annulus (m/s)
x	non-dimensional radius ($= r/b$)
z	axial co-ordinate (m)
β	swirl ratio ($= V_\phi/\Omega r$)
$\lvert\Delta\varepsilon_c\rvert$	absolute difference of concentration effectiveness between stator wall and core
ε_c	concentration effectiveness
$\lambda_{T,0}$	turbulent flow parameter ($=\dot{m}_0 Re_\Phi^{-0.8}/\mu b$)
μ	dynamic viscosity (kg/ms)
ρ	density (kg/m^3)
Φ	non-dimensional sealing parameter ($= \dot{m}/2\pi s_c\rho\Omega b^2$)
Φ_B	non-dimensional sealing parameter for bore flow ($= \dot{m}_B/2\pi s_c\rho\Omega b^2$)
Φ_L	non-dimensional sealing parameter for leakage flow ($= \dot{m}_L/2\pi s_c\rho\Omega b^2$)
Φ_0	total superposed flow sealing parameter ($= \Phi_B + \Phi_L$)
Ω	angular speed of rotating disc (rad/s)

Subscripts

a	annulus
B	bore flow
i	inner
L	leakage flow
o	outer
ref	reference
s	stator surface
0	total
∞	core

References

[1] Rolls-Royce, 2005, "The Jet Engine," 5th ed., London: Rolls-Royce plc.

[2] Cocca A. M., Stappenbeck, A., Van Wormer, J., 1996, "GE MS7001 Gas Turbine Advanced Technology Update", ASME paper 96-GT-13.

[3] Mohammed-Fakir, A-A., Safi, A., Kellock, I. R., Itzel, G. M., Arness, B. P, 2003, "Supplemental Seal for the Chordal Hinge Seals in a Gas Turbine," US Patent No.: US 6,637,753 B2.

[4] Scobie, J. A., Sangan, C. M., Owen, J. M., and Lock, G. D., 2016, "Review of Ingress in Gas Turbines," ASME J. Eng. Gas Turb. Power, 138(12), p.120801.

[5] Bunker, R. S., 2007, "Gas Turbine Heat Transfer: Ten Remaining Hot Gas Path Challenges," ASME J. Turbomach., 129(2), p.193-201.

[6] Andreini, A., Da Soghe, R., Facchini, B., 2010, "Turbine Stator Well CFD Studies: Effects of Coolant Supply Geometry on Cavity Sealing Performance," ASME J. Turbomachinery, 133(2), p.021008.

[7] Palafox, P., Ding, Z., Bailey, J., Vanduser, T., Kirtley, K., Moore, K., and Chupp, R., 2013, "A New 1.5-Stage Turbine Wheelspace Hot Gas Ingestion Rig (HGIR) – Part I: Experimental Test Vehicle, Measurement Capability and Baseline Results," ASME Paper GT2013-96020.

[8] Ding, Z., Palafox, P., Moore, K., Chupp, R., Kirtley, K., 2013, "A New 1.5-Stage Turbine Wheelspace Hot Gas Ingestion Rig (HGIR): Part II — CFD Modeling and Validation," ASME Paper GT2013-96021.

[9] Clark, K., Barringer, M., Johnson, D., Thole, K., Grover, E., Robak, C., 2017, "Effects of Purge Flow Configuration on Sealing Effectiveness in a Rotor-Stator Cavity," ASME Paper GT2017-63910.

[10] Zhang, F., Wang, X., Li, J., Zheng, D., 2017, "Numerical Investigation on the Effect of Radial Location of Sealing Air Inlet And its Geometry on the Sealing Performance of a Stator-Well Cavity," Int. J. Heat and Mass Transfer, 115(B), p.820-832.

[11] Sangan, C. M., Pountney, O. J., Zhou, K., Wilson, M., Owen, J. M., and Lock, G. D., 2013, "Experimental Measurements of Ingestion through Turbine Rim Seals. Part 1: Externally-Induced Ingress," ASME J. Turbomach., 135(2), p. 021012.

[12] Cho, G., Sangan, C. M., Owen, J. M. and Lock, G. D., 2016, "Effect of Ingress on Turbine Discs," ASME J. Eng. Gas Turb. Power, 138(4), p. 042502.

[13] Owen, J. M., Wu, K., Scobie, J. A., Sangan, C. M., Cho, G., Lock, G. D., 2014, "Use of Pressure Measurements to Determine Effectiveness of Turbine Rim Seals," ASME J. Eng. Gas Turb. Power, 137(3), p. 032510.

[14] Mear, L. I., Owen, J. M. and Lock, G. D., 2016, "Theoretical Model to Determine Effect of Ingress on Turbine Disks," ASME J. Eng. Gas Turb. Power, 138(3), p. 032502.

[15] Halila, E. E., Lenahan, D. T., & Thomas, T. T., 1982, "High Pressure Turbine Test Hardware Detailed Design Report," NASA Technical Report, NASA-CR-167955.

[16] Owen JM and Rogers RH., 1989, Flow and Heat Transfer in Rotating-Disc Systems, Vol. 1 – Rotor stator systems, Taunton: Research Studies Press Ltd.

[17] Sangan, C.M., Pountney, O.J., Scobie, J.A., Wilson, M., Owen, J.M. & Lock, G.D., 2013, "Experimental Measurements of Ingestion through Turbine Rim Seals. Part 3: Single and Double Seals," ASME J. Turbomach., 135(5), p. 051011.

[18] Childs, P. R. N., 2011, Rotating flow, Oxford: Butterworth-Heinemann.

[19] Sangan, C. M., Lalwani, Y., Owen, J. M., Lock, G. D., 2014, "Fluid Dynamics of a Gas Turbine Wheel-Space with Ingestion," IMechE Journal of Power and Energy, 228, p. 508-524.